Annals of Glaciology

Article

Cite this article: Montgomery L, Koenig L, Lenaerts JTM, Kuipers Munneke P (2020). Accumulation rates (2009–2017) in Southeast Greenland derived from airborne snow radar and comparison with regional climate models. *Annals of Glaciology* **61**(81), 225–233. https://doi.org/10.1017/aog.2020.8

Received: 31 July 2019
Revised: 29 January 2020
Accepted: 30 January 2020
First published online: 21 February 2020

Key words:
accumulation; ice-sheet mass balance; polar firn; remote sensing

Author for correspondence:
Lynn Montgomery,
E-mail: lynn.montgomery@colorado.edu

cambridge.org/aog

Accumulation rates (2009–2017) in Southeast Greenland derived from airborne snow radar and comparison with regional climate models

Lynn Montgomery[1], Lora Koenig[2], Jan T. M. Lenaerts[1] and Peter Kuipers Munneke[3]

[1]Department of Atmospheric and Oceanic Sciences, University of Colorado Boulder, Boulder, CO, USA; [2]National Snow and Ice Data Center, Cooperative Institute for Research in Environmental Studies, Boulder, CO, USA and [3]Institute for Marine and Atmospheric Research (IMAU), Utrecht University, Utrecht, The Netherlands

Abstract

Since the year 2000, Greenland ice sheet mass loss has been dominated by a decrease in surface mass balance rather than an increase in solid ice discharge. Southeast Greenland is an important region to understand how high accumulation rates can offset increasing Greenland ice sheet meltwater runoff. To that end, we derive a new 9-year long dataset (2009–17) of accumulation rates in Southeast Greenland using NASA Operation IceBridge snow radar. Our accumulation dataset derived from internal layers focuses on high elevations (1500–3000 m) because at lower elevations meltwater percolation obscured internal layer structure. The uncertainty of the radar-derived accumulation rates is 11% [using Firn Densification Model (FDM) density profiles] and the average accumulation rate ranges from 0.5 to 1.2 m w.e. With our observations spanning almost a decade, we find large inter-annual variability, but no significant trend. Accumulation rates are compared with output from two regional climate models (RCMs), MAR and RACMO2. This comparison shows that the models are underestimating accumulation in Southeast Greenland and the models misrepresent spatial heterogeneity due to an orographically forced bias in snowfall near the coast. Our dataset is useful to fill in temporal and spatial data gaps, and to evaluate RCMs where few in situ measurements are available.

Introduction

Driven by rising atmospheric temperatures, the Greenland ice sheet (GrIS) is losing mass at an accelerated rate (van den Broeke and others, 2009; Shepherd and others, 2012; Hanna and others, 2013; van Angelen and others, 2014; Kjeldsen and others, 2015; Bevis and others, 2019). The total mass loss of the GrIS over the 2010–18 period is estimated to be 286 ± 20 Gt a^{-1}, with 49 ± 3 Gt a^{-1}, coming from Southeast Greenland (Mouginot and others, 2019). In the remainder of the 21st century, it is expected that increased meltwater runoff, and the associated decrease in surface mass balance (SMB) will dominate solid ice discharge as the GrIS's largest contribution to sea level rise (e.g. Enderlin and others, 2014). SMB is defined as snow accumulation and wind-driven snow redistribution (through erosion or redeposition), minus runoff, where accumulation is the difference between snowfall and evaporation/sublimation (Lenaerts and others, 2019). In this study, we ignore redistribution, as it is two orders of magnitude smaller than snowfall integrated across Southeast Greenland (Lenaerts and others, 2012). Although it is not the focus of this study, redistribution likely explains a large portion of the small scale (<1 km) variability in accumulation (Dattler and others, 2019). Additionally, there is little-to-no-runoff expected in the period we observed between the last peak melt and mid-spring. Therefore, we assume SMB to be equal to accumulation in this study.

Southeast Greenland, which we define as the region between 45° W to 33° W and 60° N to 67° N (Fig. 1), encompasses the area with the highest accumulation rates on the GrIS (Berdahl and others, 2018; Shepherd and others, 2019). Regional climate models (RCMs) suggest that Southeast GrIS receives ~30% of the total GrIS snowfall (Miège and others, 2013). Therefore, interannual variations in this region strongly influence the total GrIS mass balance, even determining the sign of the total mass balance during some years (Burgess and others, 2010). However, evaluating the rate and pattern of accumulation in climate models is challenging, as there are very few in situ observations available on the Southeast GrIS (e.g. Ettema and others, 2009; Hanna and others, 2011; Lucas-Picher and others, 2012; van den Broeke and others, 2016; Fettweis and others, 2017; Montgomery and others, 2018).

Using airborne observations, we can address the lack of in situ accumulation observations in Southeast Greenland. A first compilation of GrIS accumulation rates derived from NASA Operation IceBridge (OIB) airborne snow radar was presented by Koenig and others (2016) for the period of 2009–12. Here, we extend the time series of radar-derived accumulation rates to 2017 focusing on Southeast Greenland, using observationally constrained, gridded firn density products to convert radar-derived depth to accumulation. In addition, we compare these radar-derived accumulations with two RCMs, the Modèle Atmosphérique Régional version 3.9 (MAR) and the Regional Atmospheric Climate Model version 2.3p2 (RACMO2).

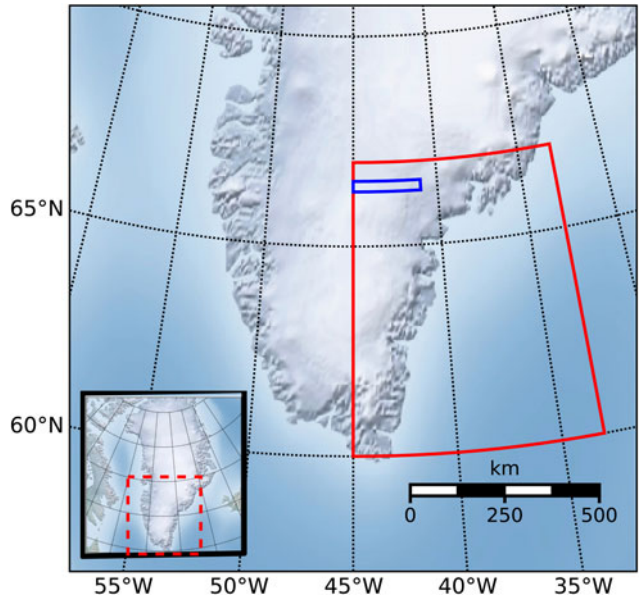

Fig. 1. Overview of our bounded study region in Southeast Greenland (red) and flight-line case study region (blue). Inlaid box is a map of Greenland with a box around the zoomed area (dashed red).

The goal of this work is to understand the magnitude, spatio-temporal variability and uncertainty of radar-derived accumulation in Southeast Greenland, and to provide an initial assessment of RCM performance in simulating Southeast Greenland SMB.

Observations, instruments and models

Operation IceBridge airborne snow radar data

From 2009 to 2019, the Center for Remote Sensing of Ice Sheets (CReSIS) at the University of Kansas operated the snow radar onboard the NASA P3-B and DC8 aircraft during OIB missions. We use the radar data from 2009 to 2017 due to data and model output availability at the time of the study. This radar maps internal annual accumulation layers ranging from 10 cm to >1 m (Panzer and others, 2013). These data, IceBridge snow radar L1B Geolocated Radar Echo Strength Profiles, Version 2, are available from the National Snow and Ice Data Center (NSIDC; Paden and others, 2014). The snow radar detects isochronal layers in the firn and are dated by assuming annual stratigraphy and counting each layer down from the surface (Medley and others, 2013; Koenig and others, 2016). Annual layering of accumulation can be detected because radar reflection horizons represent contrasts in the material's dielectric permittivity, attributed to isochronous buried sequences, ice crusts and snow layers (Medley and others, 2013). The radar uses a frequency-modulated continuous wave architecture that operates in the 2–6.5 GHz frequency range with a vertical resolution of ~5 cm (Medley and others, 2013; Panzer and others, 2013). We chose this radar over the other radars aboard OIB because of its high vertical resolution and shallower penetration depth that allow the radar to measure recent accumulation rates (past ~1 to 20 years).

In-situ density observations

The SUMup (SUrface Mass balance and snow depth on sea ice working group) dataset provides snow and firn density profiles and accumulation measurements across the entire GrIS (Montgomery and others, 2018). Density profiles from 306 locations on the GrIS are used to compare modeled with observed densities in the top meter of firn (Figs 2a and b; Renaud, 1959; Ohmura, 1991, 1992; Alley, 1999; Bolzan and Strobel, 1999*a*, 1999*b*, 1999*c*, 1999*d*, 1999*e*, 1999*f*, 1999*g*, 2001*a*, 2001*b*; Miller and Schwager, 2000*a*, 2000*b*; Wilhelms, 2000*a*, 2000*b*, 2000*c*, 2000*d*; Bales and others, 2001; Mosley-Thompson and others, 2001; Conway, 2003; Dibb and Fahnestock, 2004; Dibb and others, 2007; Mayewski and Whitlow, 2009*a*, 2009*b*, 2009*c*, 2009*d*; Harper and others, 2012; Benson, 2013, 2017; Miège and others, 2013; Hawley and others, 2014; Koenig and others, 2014; Baker, 2016; Chellman, 2016; Machguth and others, 2016; Schaller and others, 2016, 2017; Cooper and others, 2018; MacFerrin and others, 2018*a*, 2018*b*). We use 35 density profiles from Southeast Greenland to compare with RCM density in the top 5 m. Most density profiles were retrieved from firn cores (98%) with average core depths >10 m while a small fractions were taken from snow pits (2%) with depths <2 m.

MAR and RACMO2 simulated SMB

We use our radar-derived observations to evaluate the accumulation simulated by two RCMs (MAR and RACMO2) over Southeast Greenland. MAR and RACMO2 are forced at their lateral boundaries by a reanalysis dataset (ERA-Interim 1979–2018) (Noël and others, 2016; Fettweis and others, 2017; Delhasse and others, 2018). Monthly gridded SMB from MAR (originally 15 km) and RACMO2 (originally 5.5 km) is downscaled to a 1-km spatial resolution, and provide the atmospheric input used to derive density profiles (see 'Crocus and FDM modeled density' section). The RCM SMB products used here are downscaled based on the local regression to elevation from higher resolution digital elevation models (Noël and others, 2016; personal communication from Fettweis, 2019). These downscaled accumulation model products are used to compare with our radar-derived accumulation. Previous studies have shown that both MAR and RACMO2 SMB products compare well with available in situ observations on the GrIS (Fettweis and others, 2017; Noël and others, 2018), although an evaluation of Southeast GrIS has so far been hampered by the paucity of observations in that region.

Crocus and FDM modeled density

Spatially gridded density profiles are taken from two firn models, Crocus and the Firn Densification Model of the Institute for Marine and Atmospheric research Utrecht (IMAU-FDM v2.3p2) (referred to hereafter as Crocus and FDM, respectively). Crocus model output, available at a horizontal resolution of 15 km, is forced with atmospheric data and mass fluxes from MAR (Fettweis and others, 2017). Crocus is a snow model that simulates energy and mass evolution of a snow cover at a given location and provides vertical density profiles (Brun and others, 1989, 1992). The FDM model output, available at a 5.5 km spatial and 10-daily (instantaneous) temporal resolution, is a time-dependent, 1-D model that keeps track of the density and temperature in a vertical firn column, and is driven by atmospheric input originating from another RCM, RACMO2 (Kuipers Munneke and others, 2015; Ligtenberg and others, 2018). Model output prior to our study period is used to understand density differences across the GrIS since the majority of observations from SUMup are not from 2009 to 2017 (Fig. 2). Both densification models can simulate liquid water content, percolation, layer saturation and refreezing in firn. The FDM can store liquid water through capillary forces, which best simulates the processes occurring in the percolation zone in Southeast Greenland (Ligtenberg and others, 2011). The FDM densification rate in Southeast Greenland is tuned to density observations from 22 dry firn cores (Kuipers Munneke and others, 2015).

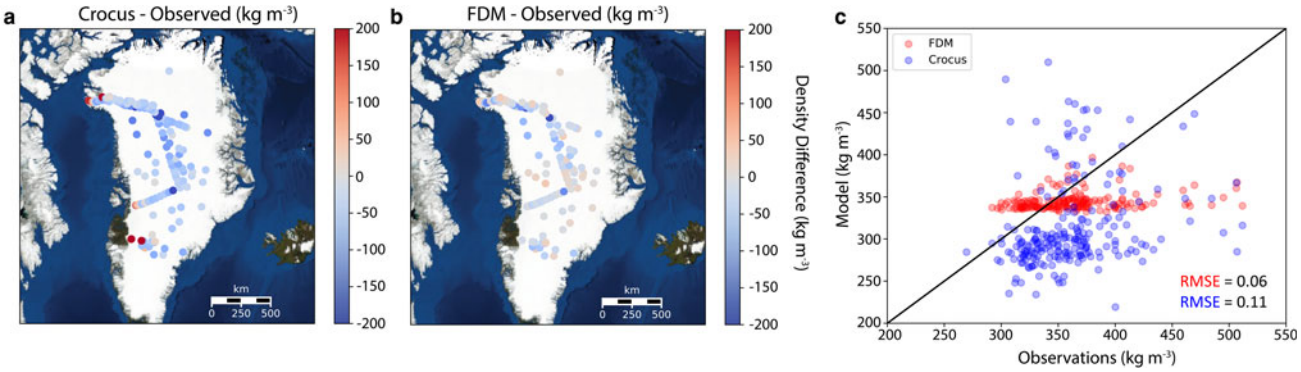

Fig. 2. Difference of average density (kg m^{-3}) in the top meter between (a) Crocus or (b) FDM and SUMup observations across Greenland. (c) Scatterplot of Crocus and FDM densities vs observations.

Methods

To derive accumulation rates ($\dot{b}$) from radar observed firn layers we use a combination of two equations following standard methods (Medley and others, 2013; Das and others, 2015; Koenig and others, 2016). Equation (1) shows the w.e. accumulation rate, $\dot{b}$, in m w.e. a^{-1} at along-track location, x, using a snow density profile, $\rho(x)$, in kg m^{-3}, with a as the age of the layer in years from the date of radar data collection, and ρ_w as the density of water in kg m^{-3}:

$$\dot{b}(x) = \frac{z(x)\rho(x)}{a(x)\rho_w} \quad (1)$$

The two way travel time of the radar (TWTT) in seconds is converted to depth, z, using a dielectric mixing model for ice–air mixture from Looyenga (1965) in Eqn (2), where c is the speed of light in m s^{-1}, ρ_i is the ice density in kg m^{-3} and ε_i' is the dielectric permittivity of pure ice:

$$z = \frac{\mathrm{TWTT}(x)\rho(x)c}{2((\rho/\rho_i)(\varepsilon_i'^{1/3} - 1) + 1)^{3/2}} \quad (2)$$

Equations (1) and (2) are combined to Eqn 3:

$$\dot{b}(x) = \frac{\mathrm{TWTT}(x)\rho(x)c}{2a(x)\rho_w((\rho/\rho_i)(\varepsilon_i'^{1/3} - 1) + 1)^{3/2}} \quad (3)$$

Selecting flight tracks

Any flight tracks that were included our study area, 45° W to 33° W and 60° N to 67° N, were downloaded from NSIDC and run through semiautomated layer picker software (detailed in Koenig and others, 2016). The flight track missions that were most often used included 'Southeast Coastal', 'Southeast Glaciers', 'Helheim-Kangerdlugssuaq', but vary depending on the year. Often, accumulation rates could not be derived because the layers were not clearly identifiable due to topography, flight maneuvers or meltwater percolation disrupting firn stratigraphy. There are no annual accumulation measurements available in SUMup coincident in space and time to compare with our new OIB-derived accumulation. Instead, radar-derived accumulation rates are directly compared with modeled accumulation, because our observations reflect all of the individual components of SMB throughout the winter season (when melt and runoff are absent), i.e. snowfall and sublimation/evaporation.

Density profiles and associated uncertainties

In Southeast Greenland, only 35 observed density profiles, $\rho(x)$, are available from SUMup. Therefore, we seek to increase the coverage of this region using the FDM and Crocus firn models that have gridded density products available. A simple model, such as a semiempirical firn densification model that assumes a dry firn column, as described by Herron and Langway (1980), cannot be used to approximate density profiles in Southeast Greenland, because it is a region where liquid water is commonly found in the firn. To assess how these models perform and which to use for our study, we compare their output against observations at corresponding times and locations. The FDM density profiles were linearly interpolated in time to find daily values, since the original data are only output every 10 days. There is no FDM model output available beyond 2016, so an average the 2009–16 density profile was used to derive accumulation for 2017, which provides a conservative estimate. If no day was associated with the measurement in the SUMup dataset, we assigned the date to be 1st May, as in Koenig and others (2016).

To determine which gridded density product to use to derive accumulation and its associated uncertainty, we examine densities from models compared with observations in the top meter and 5 m of snow across Greenland spatially. The comparison of observed and modeled density in the top meter of snow shows us how well surface processes are being represented. In the top meter across all of Greenland for 306 unique locations from the SUMup dataset (Fig. 2a), Crocus underestimates densities by 50 kg m^{-3}, similar to the results of a 60 kg m^{-3} underestimation from Alexander and others (2019). In Southeast Greenland specifically, densities are being underestimated by an average of 80 kg m^{-3} in the top meter of firn, with an average observed value of 362 ± 45 kg m^{-3} and an average Crocus output value 294 ± 29 kg m^{-3}. The FDM shows only a slight overestimation of densities within the top meter by 20 kg m^{-3} across all of Greenland (Fig. 2b). In Southeast Greenland, the FDM agrees well with observations, with densities overestimated by 30 kg m^{-3} and an average density value of 343 ± 24 kg m^{-3}. The FDM has less variability than Crocus as well as a lower root mean squared error (RMSE) (0.06 for FDM vs 0.11 for Crocus, Fig. 2c) showing that it better represents densities in the top meter of the GrIS. However, neither model is capturing small scale variation in observed densities likely due to grid resolution (Fig. 2c). Our uncertainty is defined as the absolute difference between the modeled density and observed density in the top meter, which is determined to be 19 and 5% for Crocus and FDM, respectively. We use these errors as a measure for the final radar-derived accumulation uncertainty, because this layer comprises most (if not all) of the winter accumulation.

Further, we analyze the density profiles of both observations and models to the depth of the highest radar-derived accumulation rates we have observed, ~5 m snow w.e. The average density of the top 5 m of snow/firn from SUMup observations in

Southeast Greenland (representing 35 unique cores) is 437 ± 59 kg m^{-3} (Fig. 3). Below the top meter in Crocus, the densification rate slows because there is less pore space available to compact and it is compensating for the excessive densification rate above. This compensation of density values allows Crocus to have a low bias for the top 5 m with an average value of 432 ± 90 kg m^{-3}. The FDM density profile agrees better with the observations overall, showing a similar densification rate, although it still slightly underestimates the average density values (404 ± 50 kg m^{-3}). We use the FDM density profiles to derive accumulations and in our analysis because they are within the uncertainty range of the observations, i.e. ±1 std dev., though we also derive accumulations using the Crocus profiles only to quantify the total uncertainty.

Determining layer age and total accumulation uncertainty

Depth or layer ages, a, are determined by assuming that spatially continuous isochronal layers are annually resolved. An automated layer picker (Koenig and others, 2016) was used to find the peak density gradients to determine layer ages that were verified and adjusted manually as necessary using a graphical user interface. The first layer would represent 10 months instead of the full year in our study. This is because it encompasses the springtime measurement from the snow radar aboard OIB (often taken in April/May) back to the previous year's melt, causing a peak in the density gradient in July ± 1 month (Koenig and others, 2016). The second source of error occurs during manual adjustment of the picked layers and is estimated to be a maximum of ±3 range bins, or ~8 cm (Koenig and others, 2016). In our study, this accounts for a range of 7–13% errors (10% on average) depending on accumulation rates, which is similar to the mean error of 7% found in Koenig and others (2016). Combining this with the errors from the density models we get a total error range on the radar-derived accumulation of 11% (FDM) to 21% (Crocus) depending on the firn model used. The results we show are only representative of the radar-derived accumulations using the FDM density profiles.

Results

Radar-derived accumulation rates

A time series of accumulation rates and their uncertainties were derived from OIB snow radar from 2009 to 2017 (Fig. 4). Average radar-derived accumulation across all of Southeast Greenland for each year ranges from 0.5 to 1.2 m w.e. with higher values near the coast and decreasing values as you move inland. The year-to-year variable acquisition of observations is due to the variations in flight lines and data quality. An increase in spatial coverage from 2009 to 2011 can be explained by a greater number of flights and adjustments to the radar antenna leading to better data quality (Koenig and others, 2016). Resulting from the improved data quality, the percentage of measurements that were able to be derived from all flight lines increased from ~40 to 70% in those years. From 2012 to 2014, there was less coverage, with only one flight line obtained in 2013 and three in 2014, likely due to unfavorable flying conditions in those seasons, along with only ~22–46% of the data of sufficient quality. Years 2015 and 2017 provide more complete spatial coverage, with more consistent flight paths as well as ~58–65% of the radar data containing discernible layers. In 2016, there was reduced radar performance on many flights leading to a lack of quality data (36%). The number of flights and area covered varies by year (Supplementary Table 1, Fig. 4), with peak coverage in 2011 (70%) and 2015 (65%).

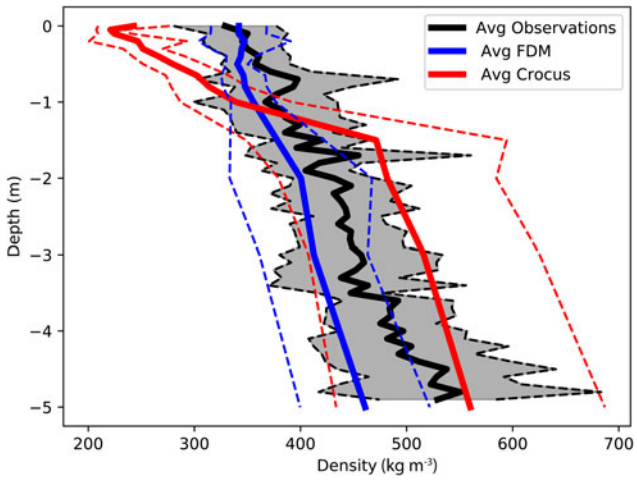

Fig. 3. Average density profile of the top 5 m of all observed SUMup ($N = 35$) cores (black) in Southeast Greenland and co-located FDM (blue), and Crocus (red) in space and time. The std dev. is shown in the dashed line of the same color.

Comparison with RCMs: interannual variability

With a dataset of radar-derived accumulation rates spanning almost 10 years, we can analyze the interannual variability and compare that with RCMs (Fig. 5). Since there is no single OIB flight line that is consistently flown every year from 2009 to 2017, we focus our analysis on an area (45° W to 41° W and 66.3° N to 66.55° N, Fig. 1) that contains a partial set of flight lines each year (except for 2009), and match these observations in space and time with the closest MAR and RACMO2 grid points. Accumulation from RACMO2 follows a similar pattern of interannual variations, although it had a relatively large bias of −0.18 m w.e (44%). In contrast, MAR shows a more constant accumulation rate from 2010 to 2017. However, its multi-annual mean is closer to the observations, with an average bias of −0.13 m w.e. (29%). Over this time period, RACMO2 captures the interannual trends ($r^2 = 0.86$) while MAR does not ($r^2 = 0.08$), showing very little interannual variability. To assess how representative the 2010–17 period is for the longer-term accumulation record (1979–2017), and considering the above model biases, we analyze the 30-year mean and variability in accumulation across the same area from RCMs (Fig. 5b). For both RACMO2 and MAR, the std dev. of the 2010–17 accumulation (RACMO2: 0.408 ± 0.039; MAR: 0.45 ± 0.024) fall within the 1979–2017 variability (RACMO2: 0.43 ± 0.063; MAR: 0.47 ± 0.068). This implies that the RCM analysis in this study area is consistent with interannual patterns spanning multiple decades.

Comparison with RCMs: spatial variability

Radar-derived accumulation rates from each 10-month period were compared with downscaled 1 km MAR and RACMO2 accumulation covering the same period. The years of 2011 and 2015 had the best spatial coverage and are shown in Figure 6i. RACMO2 underestimates accumulation rates in Southeast Greenland with a mean bias of −0.51 m w.e. across the entire region in 2011 and −0.41 m w.e. in 2015. In 2011, accumulation is overestimated toward the lower elevations (<1500 m) but this is dominated by accumulation underestimation everywhere else. MAR closely matches accumulation rates in 2011 with a mean bias of −0.09 m w.e. and in 2015 the mean bias is −0.22 m w.e. averaged across Southeast Greenland. This good agreement in 2011 reflects the low spatial heterogeneity compared with observations. Scatterplots show a similar pattern to the difference plots, showing that both MAR and RACMO2 underestimate

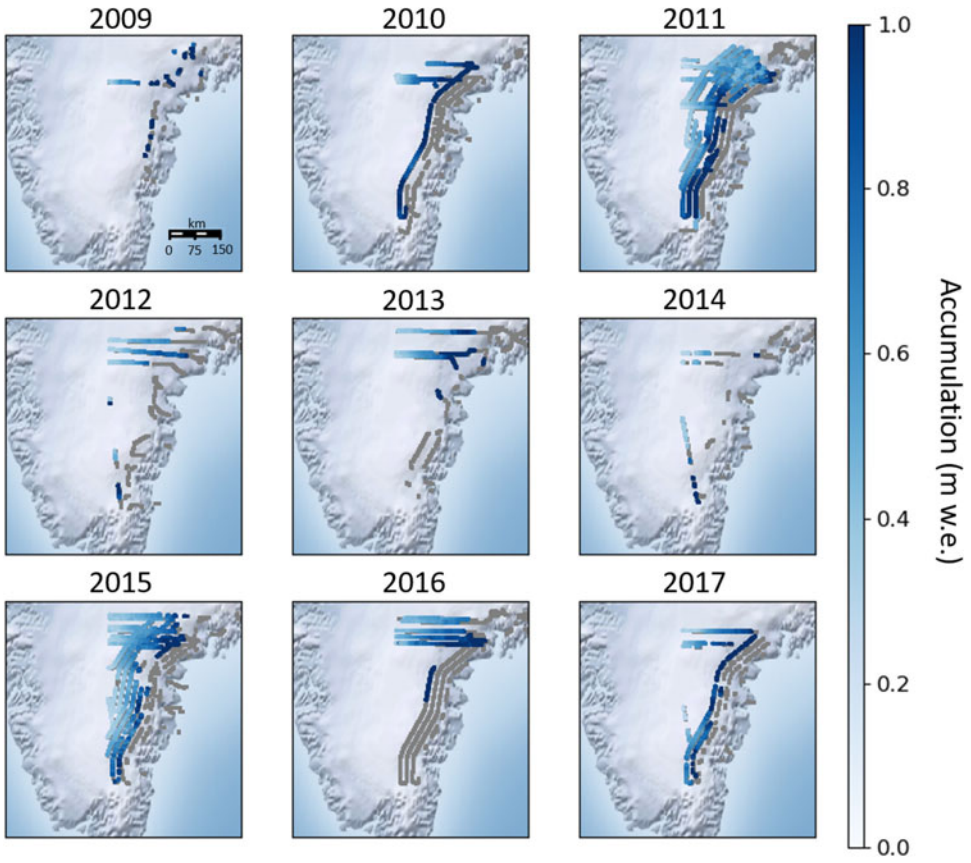

Fig. 4. Annual accumulation (m w.e.) derived from OIB snow radar, from 2009 to 2017. Flight tracks that were not discernible for accumulation layers are shown in gray.

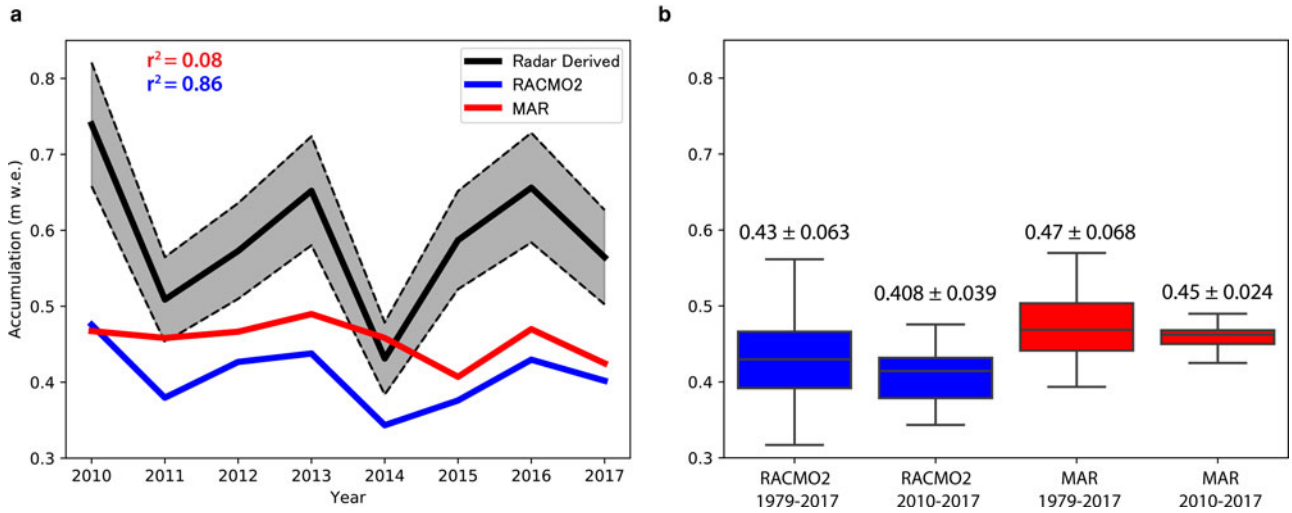

Fig. 5. (a) Inter-annual variability of radar-derived accumulation rates (black) from 2010 to 2017 of area overflown each year compared with MAR (red) and RACMO2 (blue). Uncertainty of observations (11%) shown in dashed lines of the same color. (b) Box plot of RACMO2 and MAR accumulations from 1979 to 2017 showing the middle 50% of data (second and third quartiles), the line inside the box represents the median values, and the whiskers show the greatest/least values within 1.5 times the interquartile range of the upper and lower quartiles.

accumulation in Southeast Greenland (Fig. 6ii). The RMSE for RACMO2 during 2011 (0.26) and 2015 (0.29) are greater than those from MAR for the same years (0.17 and 0.23). When considering the 11% uncertainty of the radar-derived accumulation, the RMSE of each year decreases, except for MAR in 2011 where the RMSE is the same (RACMO2 2011: 0.18, RACMO2 2015: 0.12; MAR 2011: 0.17, MAR 2015: 0.08). However, the uncertainty does not fully account for the difference in radar-derived vs modeled accumulation and therefore it must be attributed to a physical process in the models.

Discussion

Annual accumulation can be derived from OIB-airborne radar in Southeast Greenland. However, in general, only the most recent layer or ~10 months can be detected in the percolation zone

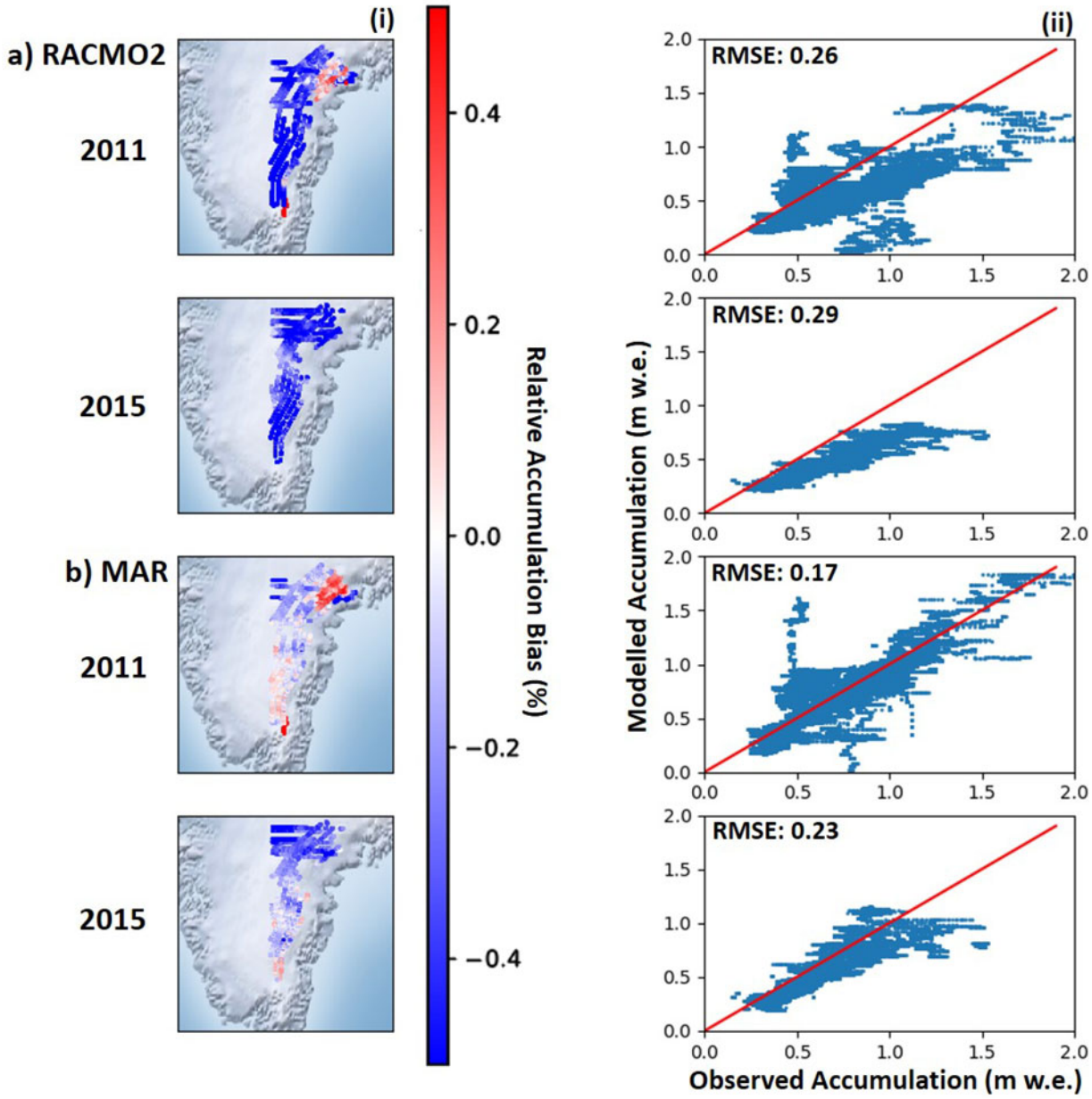

Fig. 6. (a) (i) Relative difference between OIB derived accumulation and RACMO2 for 2011 and 2015, and (ii) scatterplots showing radar-derived accumulation vs RACMO2. (b) The same analysis except with MAR.

where melt and refreezing obscures the stratigraphy below the last year's snowfall. A future increase and inland progression of surface melt on the GrIS implies that this technique's potential to yield reliable long-term accumulation records will be progressively more challenging in the future. We can reduce the spatial uncertainty of these derived measurements by attaining more in situ observations along OIB flight-line tracks.

This study provides a record of OIB radar-derived accumulation in Southeast Greenland that has been extended from Koenig and others (2016) to include 2009 to 2017. Compared with that earlier study, we have also updated some of the methods and datasets. First, we use an updated version of MAR (v3.9.2) as well as RACMO2 to compare RCM accumulation with OIB radar-derived accumulation. Second, we use FDM density profiles to derive accumulation, which best represent Southeast Greenland. The resulting differences between our results and Koenig and others (2016) illustrate that realistic density profiles are essential to convert radar-derived depth to accumulation. This is highlighted by our comparison of Crocus and FDM with observations, yielding a total uncertainty associated only with a density choice of 5% (FDM) to 19% (Crocus). The FDM density profiles show better agreement with observations, likely because the FDM physics are designed for use over ice sheets, while the Crocus model is developed for Alpine snow conditions. FDM profiles are also tuned to measurements from the GrIS (Kuipers Munneke and others, 2015). Along with the density estimate, layer picking software is a source of uncertainty in deriving accumulation rates and has been quantified by Koenig and others (2016) to be ~8 cm from manual adjustment of layers or an average of 10% uncertainty in our study. Our overall uncertainty of 11% on radar-derived accumulation is reasonable compared with other studies, which yield uncertainties of 14–15% (Medley and others, 2013; Koenig and others, 2016). The biases between models and observations as well as the uncertainties can be constrained by collecting additional coincident observations of accumulation and density in Southeast Greenland. These observations are also necessary to provide an independent estimate of Southeast Greenland accumulation, as RCMs are currently the only tool available to provide GrIS SMB at this spatial resolution.

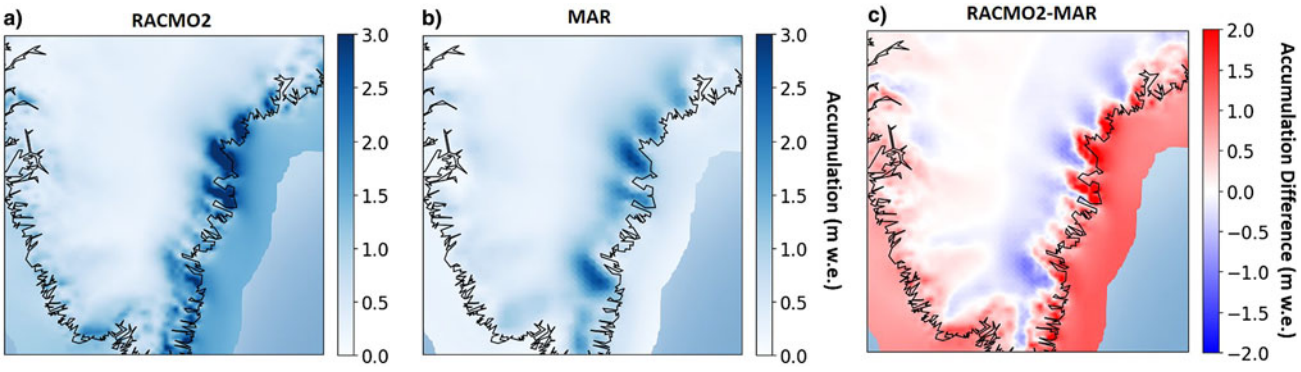

Fig. 7. Average annual snowfall (m w.e.) from 2009 to 2017 in (a) RACMO2, (b) MAR and (c) RACMO2–MAR.

To assess future changes in accumulation and SMB, we must be able to differentiate between interannual variability and longer-term trends in RCMs. Interannual variability of accumulation in Southeast Greenland is driven by synoptic patterns associated with the strength and location of the Icelandic Low situated to the east of Greenland (Berdahl and others, 2018). On average, the large-scale southwesterly atmospheric circulation brings moisture to the southern coast of Greenland, where the steep slopes of the ice sheet act as efficient barriers to the flow, and orographic precipitation is abundant. Over the 2010–17 time period (2009 is excluded because no flight lines overlap our case study region in that year), our case study shows that RACMO2 captures the interannual trends better than MAR, while MAR better represents the absolute magnitude of radar-derived accumulation. Over a 30 year period from 1979 to 2017, accumulation is examined from MAR and RACMO2 to show that variability of the study period (2010–17) is within that of the longer-term from both RCMs (Fig. 5b). On the other hand, the 8-year time period we observe is too short to discern a significant long-term trend. We would need OIB data from a longer time period, similar to that of the RCMs (>30 years), to attempt to isolate long-term trends from interannual variability.

In order to quantify how much accumulation Southeast Greenland contributes to the GrIS's total SMB, and how it may impact changes in SMB in the future, spatial variability of accumulation in RCM's is vital to understand. When comparing modeled mean bias with observations in our flight-line case study (Fig. 5a), accumulation is underestimated by both MAR and RACMO2. This result could be due to the specific to this study area chosen, and unfortunately we are unable to expand this assessment to other regions, since this is the only region that has coverage in most years. However, our comparison of the spatial variability in models and observations (Fig. 6i) suggests that this result is valid for the larger Southeast Greenland region. As other SMB components (including melt, sublimation and blowing snow redistribution) are at least two orders of magnitudes smaller than snowfall (mm vs m) in Southeast Greenland (Box and Steffen, 2001; Lenaerts and others, 2012), the biases in the RCMs must be attributed to biases in snowfall.

RACMO2 has a high snowfall bias near the coast, while MAR has a larger bias in the interior (Fig. 7). These patterns are consistent with the relative differences shown in Figure 6, where RACMO2 shows underestimation inland and MAR shows an overestimation. Our MAR results contrast with those of Koenig and others (2016), who found that an earlier version of MAR (MAR3.5.2) overestimated accumulation in all of Southeast Greenland. With updated physics (increase in the cloud life time (Fettweis and others, 2017; Delhasse and others, 2018) and employed at higher resolution (15 vs 25 km)), MARv3.9 shows good agreement across most of the region, though still slightly underestimates accumulation. The majority of the radar-derived accumulations are taken closer inland than where RACMO2 has dominant snowfall events, closer to the coast (Fig. 7). These biases are due to the fact that we are working with model accumulation downscaled to 1 km, which better resolves accumulation than the original grids, but still cannot take into account the mountainous topography in Southeast Greenland. The bias toward higher snowfall on the coast in RACMO2 is likely due to the representation of orographic precipitation in the model, i.e. when moist easterly air masses collides with coastal mountains and precipitate as they are lifted, resulting in high coastal precipitation and drier conditions further inland. RACMO2 resolves topographical features that have to do with orographic precipitation, while MAR cannot, because downscaled 1 km RACMO2 has a higher original horizontal resolution (5.5 km) than downscaled 1 km MAR (15 km).

Our results corroborate previous work, which has shown that RACMO2 overestimates accumulation at lower elevations and MAR overestimates accumulation at higher elevations. On the Q-transect on the Qagssimiut ice lobe in South Greenland, RACMO2 shows a wet bias toward the coast that is likely the dominant source of error (Hermann and others, 2018). Similarly, in RACMO2, Antarctica has a bias of orographic precipitation in coastal areas, likely because it does not compute precipitation prognostically (i.e. snow falls in the same gridcell that it is created) (Lenaerts and others, 2018). Schmidt and others (2018) emphasized the same concern about overestimation of accumulation due to high orographic forcing in RCMs and attributes some of the error to the precipitation scheme in hydrostatic models, recommending the use of WRF or HARMONIE as a non-hydrostatic alternative. Our results further verify these model biases, leading to the conclusion that RCMs must be improved to be better representative of the current climatological conditions since observations will continue to be sparse across the majority of the ice sheet. We propose future work of comparing radar-derived accumulations using a diagnostic, non-hydrostatic, high resolution model to diagnose the different precipitation schemes and see if we can reduce the error in accumulation. Additionally, we recommend that model development target orographically forced precipitation at the coast, as it is a large source of error in SMB calculations that could influence total SMB of the GrIS.

Conclusions

A dataset of annual accumulation was derived from OIB snow radar for 2009–17 in Southeast Greenland where there were very few in situ measurements available. Our estimated uncertainty of this new dataset is 11%, which results from the uncertainty associated with semiautomated layer picking software, and uncertainty in the FDM density profiles used to derive the

accumulation. We find that density profiles vary widely in the top meter of firn and can widely affect accumulation rates, especially in the high-accumulation area of Southeast Greenland. This dataset can be used to validate RCMs in Southeast Greenland, an area of high variability and uncertainty. RACMO2 consistently underestimates accumulation rates across the entire region in 2011 and 2015 (the years with the best spatial coverage), but was able to capture interannual variability in a case study region. MAR shows better agreement with accumulation rates in 2011 and 2015 across Southeast Greenland, though shows little interannual variability. The pattern observed in the relative differences can be explained by the snowfall component of each model which is biased higher toward the coast in RACMO2 and inland in MAR. In situ observations in this region will always be sparse, so we must rely on RCMs in the future to assess changing SMB. This study points to the need of focused model development of precipitation schemes to more accurately portray high accumulation regions on the GrIS.

Supplementary material. The supplementary material for this article can be found at https://doi.org/10.1017/aog.2020.8

Data. This new accumulation dataset is available at the Arctic Data Center (doi: https://doi.org/10.18739/A2J96095Z).

Acknowledgements. Lynn Montgomery and Lora Koenig acknowledge the National Science Foundation (PLR 1603407) and the NASA Earth and Space Science Fellowship (80NSSC17K0383). Peter Kuipers Munneke is funded by the Netherlands Earth System Science Centre (NESSC). We thank Xavier Fettweis for assistance with MAR model output and Brice Noël for discussion about RACMO2 output. We also thank the Associate Chief Editor Dustin Schroeder, the Scientific Editor Michelle Koutnik, and the two anonymous reviewers for their comments and suggestions, which greatly helped us in improving our paper.

References

Alexander PM, Tedesco M, Koenig LS and Fettweis X (2019) Evaluating simulated Greenland ice sheet near-surface snow and firn density in the MAR regional climate model. *Geophysical Research Letters* **46**(21), 12073–12082. doi: 10.1029/2019GL084101.

Alley RB (1999) GISP2 stratigraphy. doi: https://doi.org/10.1594/PANGAEA.56103.

Baker I (2016) NEEM firn core 2009S2 density and permeability. doi: 10.18739/A2Q88G.

Bales RC, McConnell JR, Mosley-Thompson E and Csatho B (2001) Accumulation over the Greenland ice sheet from historical and recent records. *Journal of Geophysical Research: Atmospheres* **106**(D24), 33813–33825. doi: 10.1029/2001JD900153.

Benson C (2013) Greenland snow pit and core stratigraphy (analog and digital formats). Boulder, Colorado, USA: National Snow and Ice Data Center.

Benson C (2017) Greenland snow it and core stratigraphy. Carl S. Benson Collection. Coll. 2010011. Roger G. Barry Archives and Resource Center. National Snow Data Center. (Accessed June 2017).

Berdahl M and 9 others (2018) Southeast Greenland winter precipitation strongly linked to the Icelandic low position. *Journal of Climate* **31**(11), 4483–4500. doi: 10.1175/JCLI-D-17-0622.1

Bevis M and 13 others (2019) Accelerating changes in ice mass within Greenland, and the ice sheet's sensitivity to atmospheric forcing. *PNAS* **116**(6), 1934–1939. doi: 10.1073/pnas.1806562116.

Bolzan JF and Strobel M (1999*a*) Oxygen isotope data from snowpit at GISP2 Site 13. doi: https://doi.org/10.1594/PANGAEA.55510.

Bolzan JF and Strobel M (1999*b*) Oxygen isotope data from snowpit at GISP2 Site 15. doi: https://doi.org/10.1594/PANGAEA.55511.

Bolzan JF and Strobel M (1999*c*) Oxygen isotope data from snowpit at GISP2 Site 31. doi: https://doi.org/10.1594/PANGAEA.55512.

Bolzan JF and Strobel M (1999*d*) Oxygen isotope data from snowpit at GISP2 Site 37. doi: https://doi.org/10.1594/PANGAEA.55513.

Bolzan JF and Strobel M (1999*e*) Oxygen isotope data from snowpit at GISP2 Site 51. doi: https://doi.org/10.1594/PANGAEA.55514.

Bolzan JF and Strobel M (1999*f*) Oxygen isotope data from snowpit at GISP2 Site 57. doi: https://doi.org/10.1594/PANGAEA.55515.

Bolzan JF and Strobel M (1999*g*) Oxygen isotope data from snowpit at GISP2 Site 73. doi: https://doi.org/10.1594/PANGAEA.55516.

Bolzan JF and Strobel M (2001*a*) Oxygen isotope data from snowpit at GISP2 Site 44. doi: https://doi.org/10.1594/PANGAEA.59995.

Bolzan JF and Strobel M (2001*b*) Oxygen isotope data from snowpit at GISP2 Site 571. doi: https://doi.org/10.1594/PANGAEA.59996.

Box JE and Steffen K (2001) Sublimation on the Greenland ice sheet from automated weather station observations. *Journal of Geophysical Research: Atmospheres* **106**(D24), 33965–33981. doi: 10.1029/2001JD900219.

Brun E, David P, Sudul M and Brunot G (1992) A numerical model to simulate snow-cover stratigraphy for operational avalanche forecasting. *Journal of Glaciology* **38**, 13–22. doi: 10.1017/S0022143000009552.

Brun E, Martin E, Simon V, Gendre C and Coléou C (1989) An energy and mass model of snow cover suitable for operational avalanche forecasting. *Journal of Glaciology* **35**, 333–342. doi: 10.1017/S0022143000009254.

Burgess EW and 6 others (2010) A spatially calibrated model of annual accumulation rate on the Greenland ice sheet (1958–2007). *Journal of Geophysical Research: Earth Surface* **115**(F2). doi: 10.1029/2009JF001293.

Chellman N (2016) Core Atmospheric and Snow Measurements at Summit Greenland Environmental Observatory: Snow Pit. doi: 10.18739/A2888F.

Conway H (2003) Roosevelt Island ice core density and beta count data. doi: 10.7265/N55718ZW.

Cooper MG and 6 others (2018) Direct measurements of ice density down to 1 m depth in the Greenland ice sheet ablation zone during July 2016 from shallow ice cores. In supplement to: Cooper MG et al. (accepted): Near surface meltwater storage in low-density bare ice of the Greenland ice sheet ablation zone. The Cryosphere Discussions, pp. 1–25, https://doi.org/10.5194/tc-2017-107 doi: https://doi.org/10.1594/PANGAEA.886747.

Das I, Scambos TA, Koenig LS, van den Broeke MR and Lenaerts JTM (2015) Extreme wind-ice interaction over Recovery Ice Stream, East Antarctica. *Geophysical Research Letters* **42**(19), 8064–8071. doi: 10.1002/2015GL065544.

Dattler ME, Lenaerts JTM and Medley B (2019) Significant spatial variability in radar-derived West Antarctic accumulation linked to surface winds and topography. *Geophysical Research Letters* **n/a**(n/a). doi: 10.1029/2019GL085363.

Delhasse A, Fettweis X, Kittel C, Amory C and Agosta C (2018) Brief communication: impact of the recent atmospheric circulation change in summer on the future surface mass balance of the Greenland ice sheet. *The Cryosphere* **12**(11), 3409–3418. doi: https://doi.org/10.5194/tc-12-3409-2018.

Dibb JE and Fahnestock M (2004) Snow accumulation, surface height change, and firn densification at Summit, Greenland: insights from 2 years of in situ observation. *Journal of Geophysical Research: Atmospheres* **109**(D24). doi: 10.1029/2003JD004300.

Dibb JE, Whitlow SI and Arsenault M (2007) Seasonal variations in the soluble ion content of snow at Summit. Greenland: constraints from three years of daily surface snow samples. *Atmospheric Environment* **41**(24), 5007–5019. doi: 10.1016/j.atmosenv.2006.12.010.

Enderlin EM and 5 others (2014) An improved mass budget for the Greenland ice sheet. *Geophysical Research Letters* **41**(3), 866–872. doi: 10.1002/2013GL059010.

Ettema J and 6 others (2009) Higher surface mass balance of the Greenland ice sheet revealed by high-resolution climate modeling. *Geophysical Research Letters* **36**, 12. doi: 10.1029/2009GL038110.

Fettweis X and 8 others (2017) Reconstructions of the 1900–2015 Greenland ice sheet surface mass balance using the regional climate MAR model. *The Cryosphere* **11**. doi: 10.5194/tc-11-1015-2017.

Hanna E and 12 others (2011) Greenland Ice Sheet surface mass balance 1870 to 2010 based on Twentieth Century Reanalysis, and links with global climate forcing. *Journal of Geophysical Research: Atmospheres* **116**(D24). doi: 10.1029/2011JD016387.

Hanna E and 11 others (2013) Ice-sheet mass balance and climate change. *Nature* **498**(7452), 51–59. doi: 10.1038/nature12238.

Harper J, Humphrey N, Pfeffer WT, Brown J and Fettweis X (2012) Greenland ice-sheet contribution to sea-level rise buffered by meltwater storage in firn. *Nature* **491**(7423), 240–243. doi: 10.1038/nature11566.

Hawley RL and 6 others (2014) Recent accumulation variability in northwest Greenland from ground-penetrating radar and shallow cores along the Greenland Inland Traverse. *Journal of Glaciology* **60**(220), 375–382. doi: 10.3189/2014JoG13J141.

Hermann M and 9 others (2018) Application of PROMICE Q-transect in situ accumulation and ablation measurements (2000–2017) to constrain mass balance at the southern tip of the Greenland ice sheet. *Journal of Geophysical Research: Earth Surface* **123**(6), 1235–1256. doi: 10.1029/2017JF004408.

Herron MM and Langway CC (1980) Firn densification: an empirical model. *Journal of Glaciology* **25**(93), 373–385. doi: 10.3189/S0022143000015239.

Kjeldsen KK and 15 others (2015) Spatial and temporal distribution of mass loss from the Greenland ice sheet since AD 1900. *Nature* **528**(7582), 396–400. doi: 10.1038/nature16183.

Koenig LS and 12 others (2016) Annual Greenland accumulation rates (2009–2012) from airborne snow radar. *The Cryosphere* **10**(4), 1739–1752. doi: https://doi.org/10.5194/tc-10-1739-2016.

Koenig LS, Miège C, Forster RR and Brucker L (2014) Initial in situ measurements of perennial meltwater storage in the Greenland firn aquifer. *Geophysical Research Letters* **41**(1), 81–85. doi: 10.1002/2013GL058083.

Kuipers Munneke P and 10 others (2015) Elevation change of the Greenland ice sheet due to surface mass balance and firn processes, 1960–2014. *The Cryosphere* **9**(6), 2009–2025. doi: 10.5194/tc-9-2009-2015.

Lenaerts JTM and 11 others (2018) Climate and surface mass balance of coastal West Antarctica resolved by regional climate modelling. *Annals of Glaciology* **59**(76pt1), 29–41. doi: 10.1017/aog.2017.42.

Lenaerts JTM, Medley B, van den Broeke MR and Wouters B (2019) Observing and Modeling Ice Sheet Surface Mass Balance. *Reviews of Geophysics* **57**(2), 376–420. doi: 10.1029/2018RG000622.

Lenaerts JTM, van den Broeke MR, van Angelen JH, van Meijgaard E and Déry SJ (2012) Drifting snow climate of the Greenland ice sheet: a study with a regional climate model. *The Cryosphere* **6**(4), 891–899. doi: 10.5194/tc-6-891-2012.

Ligtenberg SRM, Helsen MM and van den Broeke MR (2011) An improved semi-empirical model for the densification of Antarctic firn. *The Cryosphere* **5**(4), 809–819. doi: 10.5194/tc-5-809-2011.

Ligtenberg SRM, Kuipers Munneke P, Noël BPY and van den Broeke MR (2018) Brief communication: improved simulation of the present-day Greenland firn layer (1960–2016). *The Cryosphere* **12**(5), 1643–1649. doi: https://doi.org/10.5194/tc-12-1643-2018.

Looyenga H (1965) Dielectric constants of homogeneous mixture. *Molecular Physics* **9**(6), 501–511. doi: 10.1080/00268976500100671.

Lucas-Picher P and 5 others (2012) Very high resolution regional climate model simulations over Greenland: identifying added value. *Journal of Geophysical Research: Atmospheres* **117**, D2. doi: 10.1029/2011JD016267.

MacFerrin M and 12 others (2018*a*) Rapid expansion of Greenland's low-permeability ice slabs. *Nature* **573**(7774), 403–407. doi: 10.1038/s41586-019-1550-3.

MacFerrin M, Stevens M, Abdalati W and Waddington E (2018*b*) (In Prep) The firn compaction verification and reconnaissance (FirnCover) dataset.

Machguth H and 9 others (2016) Greenland meltwater storage in firn limited by near-surface ice formation. *Nature Climate Change* **6**(4), 390–393. doi: 10.1038/nclimate2899.

Mayewski P and Whitlow S (2009*a*) Regional survey of Greenland, 1988-snow pit data, Version 1.0. doi: 10.5065/D6154F6J.

Mayewski P and Whitlow S (2009*b*) Snow pit and ice core data from Southern Greenland, 1984, Version 1.0. doi: 10.5065/D6S180MH.

Mayewski P and Whitlow S (2009*c*) Snow pit data from Greenland summit, 1987, Version 1.0. doi: 10.5065/D63X84RQ.

Mayewski P and Whitlow S (2009*d*) Snow pit data from Greenland summit, 1989 to 1993, Version 1.0. doi: 10.5065/D6NP22KX.

Medley B and 12 others (2013) Airborne-radar and ice-core observations of annual snow accumulation over Thwaites Glacier, West Antarctica confirm the spatiotemporal variability of global and regional atmospheric models. *Geophysical Research Letters* **40**(14), 3649–3654. doi: 10.1002/grl.50706.

Miège C and 6 others (2013) Southeast Greenland high accumulation rates derived from firn cores and ground-penetrating radar. *Annals of Glaciology* **54**(63), 322–332. doi: 10.3189/2013AoG63A358.

Miller H and Schwager M (2000*a*) Density of ice core ngt42C95.2 from the North Greenland Traverse. doi: https://doi.org/10.1594/PANGAEA.57655.

Miller H and Schwager M (2000*b*) Density of ice core ngt37C95.2 from the North Greenland Traverse. doi: https://doi.org/10.1594/PANGAEA.57798.

Montgomery L, Koenig L and Alexander P (2018) The SUMup dataset: compiled measurements of surface mass balance components over ice sheets and sea ice with analysis over Greenland. *Earth System Science Data* **10** (4), 1959–1985. doi: https://doi.org/10.5194/essd-10-1959-2018.

Mosley-Thompson E and 8 others (2001) Local to regional-scale variability of annual net accumulation on the Greenland ice sheet from PARCA cores. *Journal of Geophysical Research: Atmospheres* **106**(D24), 33839–33851. doi: 10.1029/2001JD900067.

Mouginot J, Rignot E, Bjørk AA, Broeke M Van Den, Millan R, Morlighem M, Noël B, Scheuchl B and Wood M (2019) Forty-six years of Greenland Ice Sheet mass balance from 1972 to 2018. *PNAS* **116**(19), 9239–9244. doi: 10.1073/pnas.1904242116.

Noël B (2016) A daily, 1 km resolution data set of downscaled Greenland ice sheet surface mass balance (1958–2015). *The Cryosphere* **17**.

Noël B and 11 others (2018) Modelling the climate and surface mass balance of polar ice sheets using RACMO2 – Part 1: Greenland (1958–2016). *The Cryosphere* **12**(3), 811–831. doi: https://doi.org/10.5194/tc-12-811-2018.

Ohmura A (1991) ETH Greenland Expedition I, progress report no. 1, April 1989 to February, 1991. Tech. Report, Department of Geography, ETH Zürich, 108 pp.

Ohmura A (1992) ETH Greenland Expedition II, progress Rep. 2, April 1991 to October, 1992. Tech. Report, Department of Geography, ETH Zürich, 94 pp.

Paden J, Leuschen C, Rodriguez-Morales F and Hale R (2014) IceBridge snow radar L1B geolocated radar echo strength profiles, Version 2. doi: 10.5067/faztwp500v70.

Panzer B and 8 others (2013) An ultra-wideband, microwave radar for measuring snow thickness on sea ice and mapping near-surface internal layers in polar firn. *Journal of Glaciology* **59**(214), 244–254. doi: 10.3189/2013JoG12J128.

Renaud A (1959) Etude physiques et chimiques sur la glace de l'indlandsis du Groenland. *Meddelelser om Groenland* **2**(177), 100–107.

Schaller CF and 5 others (2016) A representative density profile of the North Greenland snowpack. *The Cryosphere* **10**(5), 1991–2002. doi: https://doi.org/10.5194/tc-10-1991-2016.

Schaller CF, Kipfstuhl S, Steen-Larsen H-C, Freitag J and Eisen O (2017) Spatial variability of density stratigraphy and melt features for two polar snowpacks in Greenland and East Antarctica. doi: https://doi.org/10.1594/PANGAEA.884003.

Schmidt LS and 5 others (2018) Sensitivity of glacier runoff to winter snow thickness investigated for Vatnajökull Ice Cap, Iceland, using numerical models and observations. *Atmosphere* **9**(11), 450. doi: 10.3390/atmos9110450.

Shepherd A and 46 others (2012) A reconciled estimate of ice-sheet mass balance. *Science* **338**(6111), 1183–1189. doi: 10.1126/science.1228102.

Shepherd A and 89 others (2019) Mass balance of the Greenland ice sheet from 1992 to 2018. *Nature*. doi: 10.1038/s41586-019-1855-2.

van Angelen JH, van den Broeke MR, Wouters B and Lenaerts JTM (2014) Contemporary (1960–2012) evolution of the climate and surface mass balance of the Greenland ice sheet. *Surveys in Geophysics* **35**(5), 1155–1174. doi: 10.1007/s10712-013-9261-z.

van den Broeke M and 8 others (2009) Partitioning recent Greenland mass loss. *Science* **326**(5955), 984–986. doi: 10.1126/science.1178176.

van den Broeke MR and 7 others (2016) On the recent contribution of the Greenland ice sheet to sea level change. *The Cryosphere* **10**(5), 1933–1946. doi: https://doi.org/10.5194/tc-10-1933-2016.

Wilhelms F (2000*a*) Density of ice core ngt03C93.2 from the North Greenland Traverse. doi: https://doi.org/10.1594/PANGAEA.56560.

Wilhelms F (2000*b*) Density of ice core ngt14C93.2 from the North Greenland Traverse. doi: https://doi.org/10.1594/PANGAEA.56615.

Wilhelms F (2000*c*) Density of ice core ngt06C93.2 from the North Greenland Traverse. doi: https://doi.org/10.1594/PANGAEA.57153.

Wilhelms F (2000*d*) Density of ice core ngt27C94.2 from the North Greenland Traverse. doi: https://doi.org/10.1594/PANGAEA.57296.